Journal of Sound and Vibration 640 (2026) 119901

Contents lists available at ScienceDirect

Journal of Sound and Vibration

journal homepage: www.elsevier.com/locate/jsvi

On the limitations of inverse force estimation with strain-based sensing and reduced modal models in hydroelastic systems

Christof Van Zijl *, Jovana Jovanova , Apostolos Grammatikopoulos

Faculty of Mechanical Engineering, Delft University of Technology, Mekelweg 2, Delft, 2628 CD, The Netherlands

ARTICLE INFO

Keywords:
Hydroelasticity
Inverse load estimation
Strain sensing
Identifiability
Uniqueness
Modal coupling
Rigid-body modes

ABSTRACT

Inverse methods are commonly used to estimate external forces on structures when direct measurements are impractical, such as wave loading on marine structures. However, all inverse estimation approaches implicitly assume that the available measurements contain sufficient information to uniquely identify the force components of interest. The present investigation demonstrates that this assumption can be violated in a commonly adopted hydroelastic modelling framework, in which excitation forces are represented in a dry structural modal basis that includes rigid-body modes.

Using a simplified hydroelastic system as a controlled example, it is demonstrated that when strain-based sensing is combined with a modal force representation that includes rigid-body modes, the resulting inverse problem can become non-identifiable. Although rigid-body motion produces negligible strain directly, hydroelastic coupling allows rigid-body forces to induce flexible deformation, causing rigid-body and flexible force components to excite overlapping strain-response subspaces. As a result, distinct force distributions cannot, in general, be uniquely separated from strain measurements alone.

The analysis shows that acceleration-based inversion is globally ill-conditioned at low frequencies, while strain-based inversion is affected by a persistent near-null subspace associated with rigid-body modes. Regularization is used here as an illustrative mechanism for probing the inverse problem: it stabilizes the solution by suppressing poorly observable directions, but cannot recover force components aligned with them, leading to bias. Modal truncation removes these directions but yields force estimates that represent equivalent forcing within a reduced subspace rather than physical modal forces. Mixed strain-acceleration sensing improves estimation of flexible components, but rigid-body components remain sensitive to low-frequency ill-conditioning.

These results demonstrate that the identifiability of modal force components is governed by the interaction between the chosen force representation, sensing type, and hydroelastic coupling. The findings therefore establish a general limitation of inverse force estimation in coupled fluid-structure systems, independent of the specific estimation method used.

1. Introduction

In many engineering systems, we can readily observe how a structure responds, yet have limited knowledge of the forces that drive these responses. A practical alternative is to use the structure itself as a sensor— inferring the external forces from measured

* Corresponding author.
E-mail address: c.m.vanzijl@tudelft.nl (C. Van Zijl).

https://doi.org/10.1016/j.jsv.2026.119901
Received 27 October 2025; Received in revised form 23 April 2026; Accepted 18 May 2026
Available online 19 May 2026

structural responses, such as accelerations or strains, using a dynamic model of the system. Inverse problems are common in structural engineering [1], and in recent years have also become increasingly important for understanding complex loading scenarios that cannot be measured directly, such as fluid-structure interaction, where waves forces act as spatially distributed pressures over a time-varying interface [2,3].

Inverse force estimation is inherently challenging because it is often ill-posed or ill-conditioned [4,5]. At low frequencies, force estimates obtained from acceleration measurements are well known to suffer from poor conditioning. Specifically, acceleration responses scale quadratically with frequency, leading to strong amplification of measurement noise in the inverse problem. This issue is particularly relevant in hydroelastic systems, where external loading is often dominated by low-frequency wave excitation and rigid-body motion. In this context, strain-based sensing, or combinations of strain and acceleration measurements, offer a natural alternative [6,7]. Because strain is related to spatial derivatives of displacement rather than time derivatives, the corresponding force-response relationship does not exhibit the same frequency-dependent scaling, and is therefore often expected to behave more favourably in low-frequency regimes [8].

However, this intuition does not necessarily hold in hydroelastic systems. Coupled fluid-structure models are commonly expressed in a dry structural modal basis, in which excitation forces are associated with the structural modes [9–11]. For structures that also exhibit rigid-body motion, this representation includes rigid-body modes alongside flexible modes. Under hydroelastic coupling, rigid-body motion can induce structural strain through interaction with flexible modes. As a result, rigid-body and flexible force components can excite overlapping strain subspaces, and their contributions cannot, in general, be uniquely separated from strain measurements alone. This leads to a fundamentally non-identifiable inverse problem, in which multiple force distributions can produce indistinguishable structural responses.

A wide range of inverse estimation techniques have been developed to stabilize ill-posed or ill-conditioned force estimation problems, including regularization methods, state-space estimators, and Bayesian approaches [12–14], as well as more recent developments addressing uncertainty, multi-objective formulations, and sensor placement [15–17]. While these advances have improved robustness in many applications, they do not remove a fundamental prerequisite: the available measurements must contain sufficient information to uniquely identify the force components of interest. If this condition is not satisfied, no estimator—regardless of its formulation—can recover the missing information.

The central contribution of this work is to demonstrate that, when wave forces are represented in a dry modal basis that includes rigid-body modes, strain-based inverse formulations can become fundamentally non-identifiable. In this setting, rigid-body and flexible force components can excite overlapping strain subspaces, preventing their unique separation from strain measurements alone. This limitation arises from the structure of the forward operator and persists independently of the inverse method.

To isolate and analyse this mechanism, a simplified hydroelastic system is used as a controlled example. The purpose of this model is not to represent a specific application in detail, but to expose the underlying structure of the inverse problem. Within this setting, the effects of sensing type, hydroelastic coupling, regularization, and modal truncation are examined in the frequency domain. Regularization is considered here as an illustrative tool for probing the behaviour of the inverse problem: it stabilizes the solution by attenuating poorly observable directions, but does not resolve the underlying lack of identifiability associated with the forward operator.

The remainder of this paper is organized as follows. Section 2 introduces the hydroelastic modelling framework and formulates the inverse force estimation problem. Section 3 presents a numerical hydroelastic beam model that is used as an illustrative example. Section 4 presents and discusses the results of the inverse force estimation study.

2. Mathematical formulation

This section introduces the hydroelastic formulation and the forward operators that map modal excitation forces to measured responses. The objective is to analyse how the structure of the forward operator governs conditioning and, more importantly, the identifiability of modal force components.

The theoretical framework is summarized schematically in Fig. 1. Starting from the hydroelastic model (Section 2.1), the forward operator is constructed and analysed using a singular-value decomposition (Section 2.2). The singular values quantify conditioning, with small values leading to noise amplification and increased estimation variance, while the associated right singular vectors define the modal force directions that are observable from the measurements.

This analysis is used to examine the central limitation addressed in this work: when wave forces are represented in a dry modal basis that includes rigid-body modes, strain-based measurements can lead to fundamental non-identifiability. In the presence of hydroelastic coupling, the singular directions associated with small singular values may contain mixed rigid-body and flexible components, so that poorly observable directions correspond to coupled force patterns rather than purely rigid-body modes. As a result, rigid-body and flexible forces cannot be uniquely separated from strain measurements alone.

Regularization and modal truncation are then interpreted within this framework (Section 2.3). Both act by modifying or removing contributions from poorly observable directions, reducing variance at the cost of introducing bias, but neither resolves the underlying identifiability limitation imposed by the forward operator.

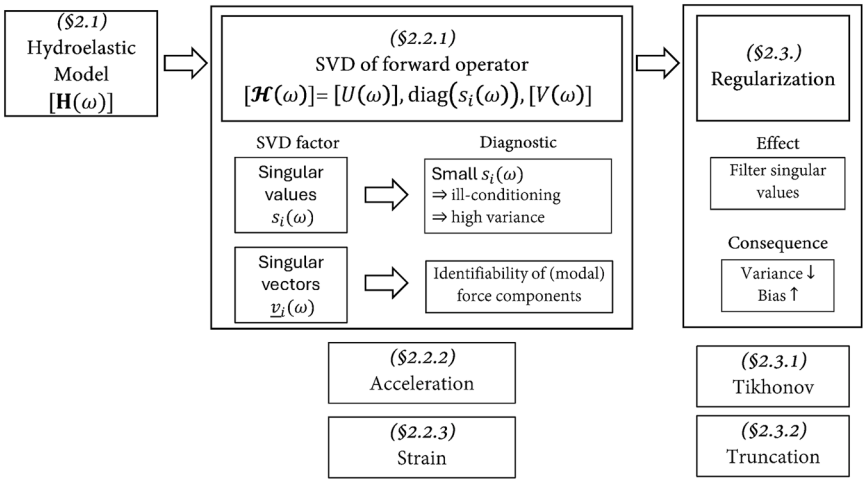

Fig. 1. Schematic overview of the theoretical framework presented in Section 2. Starting from the hydroelastic model, the forward operator is constructed and analysed using a singular-value decomposition (SVD). The singular values quantify conditioning (small values ⇒ noise amplification and high variance), while the singular vectors define the modal force directions that are observable from the measurements and therefore determine identifiability. Regularization modifies the contribution of these directions by filtering small singular values, reducing variance at the cost of introducing bias. The influence of measurement type (acceleration or strain) enters through the structure of the forward operator and its singular-value decomposition.

2.1. Hydroelastic model

The hydroelastic system is formulated in modal coordinates by projecting the structural and hydrodynamic operators onto a dry structural modal basis. The modal basis is written as

$$[\mathbf{\Phi}] = [[\mathbf{\Phi}_R][\,\mathbf{\Phi}_F\,]], \tag{1}$$

where $[\mathbf{\Phi}_R]$ and $[\mathbf{\Phi}_F]$ denote rigid-body and flexible mode shapes, respectively. The structural mass $[\mathbf{M_s}]$, damping $[\mathbf{C_s}]$, and stiffness $[\mathbf{K_s}]$ matrices are obtained from a dry structural model and expressed in these modal coordinates. The hydrodynamic contributions, consisting of the added mass $[\mathbf{M}_h(\omega)]$, radiation damping $[\mathbf{C}_h(\omega)]$, and hydrostatic stiffness $[\mathbf{K}_h]$, are projected onto the same basis.

External loading is represented in this basis through modal excitation forces $\underline{P}(\omega)$, partitioned as $\underline{P} = [\underline{P}_R^T \;\; \underline{P}_F^T]^T$. The resulting modal responses, $\underline{Q}(\omega)$ are calculated using,

$$\underline{Q}(\omega) = [\mathbf{H}(\omega)]\,\underline{P}(\omega), \tag{2}$$

where the modal frequency response function is defined as

$$[\mathbf{H}(\omega)] = \left(-\omega^2([\mathbf{M_s}] + [\mathbf{M_h}(\omega)]) + i\omega([\mathbf{C_s}] + [\mathbf{C_h}(\omega)]) + ([\mathbf{K_s}] + [\mathbf{K_h}])\right)^{-1}. \tag{3}$$

The modal frequency response function is partitioned as

$$[\mathbf{H}(\omega)] = \begin{bmatrix} [\mathbf{H}_{RR}(\omega)] & [\mathbf{H}_{RF}(\omega)] \\ [\mathbf{H}_{FR}(\omega)] & [\mathbf{H}_{FF}(\omega)] \end{bmatrix}, \tag{4}$$

where the subscripts R and F denote rigid-body and flexible components.

2.2. Analysis of forward operator

The measured response is written as

$$\underline{Y}(\omega) = [\mathcal{H}(\omega)]\underline{P}(\omega) + \underline{\mathcal{E}}(\omega), \tag{5}$$

where $[\mathcal{H}(\omega)]$ maps modal forces to measured responses. $\underline{\mathcal{E}}(\omega)$ denotes additive measurement noise, which is assumed zero-mean with covariance

$$\mathbb{E}[\underline{\mathcal{E}}(\omega)] = \underline{0}, \qquad \mathrm{Var}(\underline{\mathcal{E}}(\omega)) = \sigma^2[\mathbf{I}]. \tag{6}$$

2.2.1. Singular-value decomposition as a diagnostic tool

To analyse identifiability, the forward operator is decomposed as

$$[\mathcal{H}(\omega)] = [\mathbf{U}(\omega)]\,\mathrm{diag}(s_i(\omega))\,[\mathbf{V}(\omega)]^H = \sum_i s_i(\omega)\,\underline{u}_i(\omega)\,\underline{v}_i(\omega)^H, \tag{7}$$

The singular values $s_i(\omega)$ quantify the sensitivity of the measurements to different modal force directions. If $s_i(\omega) = 0$, the corresponding force pattern $\underline{v}_i(\omega)$ produces no measured response and is not identifiable. If $s_i(\omega)$ is small, the corresponding direction is weakly observable and highly sensitive to noise. Thus, the singular values identify poorly observable directions, while the right singular vectors specify the associated modal force patterns.

In the absence of coupling (i.e. when $[\mathbf{H}_{RF}] = [\mathbf{H}_{FR}] = [\mathbf{0}]$), the modal FRF is block-diagonal and rigid-body and flexible contributions remain separated in the singular directions. When coupling is present, however, a force applied in one mode can generate response in other modes, so the singular directions need not remain separated and may involve both rigid-body and flexible modal forces.

The unregularized estimate is

$$\underline{\hat{P}}(\omega) = \sum_i \frac{1}{s_i(\omega)} \underline{v}_i(\omega)\, \underline{u}_i(\omega)^H \underline{Y}(\omega), \tag{8}$$

with variance

$$\mathrm{Var}(\underline{\hat{P}}(\omega)) = \sigma^2 [\mathbf{V}(\omega)]\, \mathrm{diag}\left(\frac{1}{s_i^2(\omega)}\right) [\mathbf{V}(\omega)]^H = \sigma^2 \sum_i \frac{1}{s_i^2(\omega)} \underline{v}_i(\omega) \underline{v}_i(\omega)^H. \tag{9}$$

Thus, small singular values lead directly to large estimation variance along the corresponding force directions.

Moreover, assuming that the forward model is exact and the measurement noise is zero-mean, the unregularized estimate is unbiased,

$$\mathbb{E}[\underline{\hat{P}}(\omega)] = \underline{P}(\omega). \tag{10}$$

2.2.2. Acceleration-based sensing

For acceleration measurements the forward operator is given by,

$$[\mathcal{H}_a(\omega)] = -\omega^2 [\mathbf{S}_a][\mathbf{T}_x][\mathbf{\Phi}][\mathbf{H}(\omega)]. \tag{11}$$

where $[\mathbf{H}(\omega)]$ is the modal frequency response function defined in Eq. 3. The matrix $[\mathbf{T}_x]$ selects the translational degrees of freedom from the mode shape matrix $[\mathbf{\Phi}]$, while $[\mathbf{S}_a]$ selects the measured acceleration locations from the complete set of translational degrees of freedom. The acceleration operator introduces a uniform factor ω^2, so all singular values decay as $\omega \to 0$. The resulting loss of identifiability is therefore global, affecting all modal force directions equally.

2.2.3. Strain-based sensing

The forward operator for strain measurements is given by,

$$[\mathcal{H}_\varepsilon(\omega)] = [\mathbf{S}_\varepsilon][\mathbf{B}][\mathbf{\Phi}][\mathbf{H}(\omega)]. \tag{12}$$

Here, $[\mathbf{H}(\omega)]$ is the modal frequency response function defined in Eq. 3 and $[\mathbf{\Phi}]$ is the mode shape matrix that maps modal coordinates to physical coordinates. The matrix $[\mathbf{B}]$ is the strain–displacement matrix, which transforms translational and rotational degrees of freedom into strain, while $[\mathbf{S}_\varepsilon]$ selects the measured strain locations from the full strain field. Partitioning the modal FRF, the strain operator can be written as

$$[\mathcal{H}_\varepsilon(\omega)] = [\mathbf{S}_\varepsilon]\begin{bmatrix}[\mathbf{B}][\mathbf{\Phi}_R] & [\mathbf{B}][\mathbf{\Phi}_F]\end{bmatrix} \begin{bmatrix}[\mathbf{H}_{RR}(\omega)] & [\mathbf{H}_{RF}(\omega)] \\ [\mathbf{H}_{FR}(\omega)] & [\mathbf{H}_{FF}(\omega)]\end{bmatrix}. \tag{13}$$

Since $[\mathbf{B}][\mathbf{\Phi}_R] \approx [\mathbf{0}]$ (pure rigid body modes produce zero strain), this reduces to

$$[\mathcal{H}_\varepsilon(\omega)] \approx [\mathbf{S}_\varepsilon]\begin{bmatrix}[\mathbf{B}][\mathbf{\Phi}_F][\mathbf{H}_{FR}(\omega)] & [\mathbf{B}][\mathbf{\Phi}_F][\mathbf{H}_{FF}(\omega)]\end{bmatrix}. \tag{14}$$

For notational convenience, define

$$[\mathcal{H}_R(\omega)] := [\mathbf{S}_\varepsilon][\mathbf{B}][\mathbf{\Phi}_F][\mathbf{H}_{FR}(\omega)], \qquad [\mathcal{H}_F(\omega)] := [\mathbf{S}_\varepsilon][\mathbf{B}][\mathbf{\Phi}_F][\mathbf{H}_{FF}(\omega)]. \tag{15}$$

Then

$$[\mathcal{H}_\varepsilon(\omega)] = \begin{bmatrix}[\mathcal{H}_R(\omega)] & [\mathcal{H}_F(\omega)]\end{bmatrix}. \tag{16}$$

Reference: uncoupled case. If $[\mathbf{H}_{FR}] = [\mathbf{0}]$, then $[\mathcal{H}_R] = [\mathbf{0}]$, and

$$[\mathcal{H}_\varepsilon] = \begin{bmatrix}[\mathbf{0}] & [\mathcal{H}_F]\end{bmatrix}. \tag{17}$$

To identify which force patterns are associated with small singular values, we analyse the matrix

$$[\mathcal{H}_\varepsilon]^H [\mathcal{H}_\varepsilon]. \tag{18}$$

Using the singular value decomposition

$$[\mathcal{H}_\varepsilon] = [\mathbf{U}]\, \mathrm{diag}(s_i)\, [\mathbf{V}]^H, \tag{19}$$

it follows that

$$[\mathcal{H}_\varepsilon]^H[\mathcal{H}_\varepsilon] = [\mathbf{V}]\,\mathrm{diag}(s_i^2)\,[\mathbf{V}]^H, \tag{20}$$

so that the right singular vectors $\underline{v}_i$ are eigenvectors of $[\mathcal{H}_\varepsilon]^H[\mathcal{H}_\varepsilon]$ with eigenvalues s_i^2. Each $\underline{v}_i$ therefore represents a modal force pattern, and s_i quantifies how strongly this pattern is expressed in the measurements.

In the uncoupled case,

$$[\mathcal{H}_\varepsilon]^H[\mathcal{H}_\varepsilon] = \begin{bmatrix} [\mathbf{0}] & [\mathbf{0}] \\ [\mathbf{0}] & [\mathcal{H}_F]^H[\mathcal{H}_F] \end{bmatrix}. \tag{21}$$

Consider an eigenvector

$$\underline{v} = \begin{bmatrix} \underline{v}_R \\ \underline{v}_F \end{bmatrix}. \tag{22}$$

The eigenvalue problem

$$[\mathcal{H}_\varepsilon]^H[\mathcal{H}_\varepsilon]\,\underline{v} = s^2\,\underline{v} \tag{23}$$

gives

$$\underline{0} = s^2\,\underline{v}_R, \tag{24}$$

$$[\mathcal{H}_F]^H[\mathcal{H}_F]\,\underline{v}_F = s^2\,\underline{v}_F. \tag{25}$$

Thus, in the uncoupled case:

- zero singular values correspond to purely rigid-body force patterns,
- nonzero singular values correspond to purely flexible modal forces.

Rigid-body modes are therefore intrinsically unidentifiable from strain measurements, while flexible components remain identifiable provided $[\mathcal{H}_F]$ is well conditioned.

Coupled case. If $[\mathbf{H}_{FR}] \neq [\mathbf{0}]$, then

$$[\mathcal{H}_\varepsilon] = \begin{bmatrix} [\mathcal{H}_R] & [\mathcal{H}_F] \end{bmatrix}, \tag{26}$$

and

$$[\mathcal{H}_\varepsilon]^H[\mathcal{H}_\varepsilon] = \begin{bmatrix} [\mathcal{H}_R]^H[\mathcal{H}_R] & [\mathcal{H}_R]^H[\mathcal{H}_F] \\ [\mathcal{H}_F]^H[\mathcal{H}_R] & [\mathcal{H}_F]^H[\mathcal{H}_F] \end{bmatrix}. \tag{27}$$

The off-diagonal terms couple the rigid-body and flexible components in the eigenvalue problem, so that no general separation between $\underline{v}_R$ and $\underline{v}_F$ can be made. As a result, the singular directions need not remain purely rigid-body or purely flexible, and mixed directions may occur.

Small singular values arise when columns of the forward-operator blocks $[\mathcal{H}_R]$ and $[\mathcal{H}_F]$ become nearly linearly dependent, so that certain combinations of rigid-body and flexible modal forces produce similar strain responses. Equivalently, the strain-response subspaces generated by rigid-body and flexible forcing overlap. In this case, the corresponding singular directions represent coupled force patterns, and rigid-body and flexible modal forces cannot be uniquely separated from strain measurements alone. This shows that identifiability is not determined solely by the sensing type, but by the interaction between the sensing operator and the coupled modal representation.

2.3. Effect of regularization

Regularization is introduced here to clarify how the ill-conditioned directions identified above are modified in the inverse estimate. In particular, the singular-value structure shows which force patterns are attenuated by regularization and therefore where bias is introduced in exchange for variance reduction. Two types of regularization strategies are considered, namely Tikhonov regularization and modal truncation.

2.3.1. Tikhonov regularization

Tikhonov regularization yields a force estimate,

$$\underline{\hat{P}}_\lambda(\omega) = \sum_i \frac{s_i(\omega)}{s_i^2(\omega) + \lambda^2}\,\underline{v}_i(\omega)\,\underline{u}_i(\omega)^H\,\underline{Y}(\omega). \tag{28}$$

The expected value of the regularized estimate is

$$\mathbb{E}[\underline{\hat{P}}_\lambda(\omega)] = \sum_i \frac{s_i^2(\omega)}{s_i^2(\omega) + \lambda^2}\,\underline{v}_i(\omega)\,\underline{v}_i(\omega)^H\,\underline{P}(\omega), \tag{29}$$

which shows that the estimate is biased, with attenuation along directions associated with small singular values. The corresponding variance is

$$\mathrm{Var}(\underline{\hat{P}}_{\lambda}(\omega)) = \sigma^2 \sum_i \left(\frac{s_i(\omega)}{s_i^2(\omega) + \lambda^2} \right)^2 \underline{v}_i(\omega)\, \underline{v}_i(\omega)^H, \tag{30}$$

which is reduced compared to the unregularized case, particularly along directions with small singular values. Thus, Tikhonov regularization reduces variance at the cost of introducing bias.

For acceleration-based sensing, all singular directions are attenuated in a similar way at low frequencies, so regularization introduces bias across all force components. For strain-based sensing in the uncoupled case, the small-singular-value directions correspond to rigid-body forces. Regularization therefore suppresses these directions, while flexible modal forces are only weakly affected provided their singular values are sufficiently large relative to the regularization parameter.

In the coupled case, however, the small-singular-value directions contain both rigid-body and flexible components. Regularization therefore attenuates these combined directions, introducing bias into the estimated flexible modal forces.

2.3.2. Modal truncation

Modal truncation is considered as an alternative regularization strategy in which rigid-body modes are removed from the inverse formulation. The resulting estimate is restricted to the retained (flexible) subspace and is given by

$$\underline{\hat{P}}_F(\omega) = [\mathcal{H}_F(\omega)]^{\dagger} \underline{Y}(\omega). \tag{31}$$

This modification alters both the variance and bias of the estimate. Since the truncated formulation no longer attempts to invert directions associated with the removed modes, the variance is reduced relative to the full problem. However, this comes at the cost of restricting the solution space, so that components of the true force lying outside the retained subspace cannot be represented explicitly. To understand the implications, it is useful to distinguish between the uncoupled and coupled cases.

Uncoupled case. If $[\mathbf{H}_{FR}] = [\mathbf{0}]$, the measured response depends only on the flexible modal forces,

$$\underline{Y}(\omega) = [\mathcal{H}_F(\omega)]\underline{P}_F(\omega) + \underline{\mathcal{E}}(\omega), \tag{32}$$

so that the truncated estimate recovers the flexible components exactly,

$$\mathbb{E}[\underline{\hat{P}}_F(\omega)] = \underline{P}_F(\omega). \tag{33}$$

In this case, modal truncation removes only non-identifiable directions and does not introduce bias.

Coupled case. When hydroelastic coupling is present, $[\mathbf{H}_{FR}] \neq [\mathbf{0}]$, and the measured response depends on both rigid-body and flexible forces,

$$\underline{Y}(\omega) = [\mathcal{H}_R(\omega)]\underline{P}_R(\omega) + [\mathcal{H}_F(\omega)]\underline{P}_F(\omega) + \underline{\mathcal{E}}(\omega). \tag{34}$$

Substituting into the truncated estimate gives

$$\mathbb{E}[\underline{\hat{P}}_F(\omega)] = \underline{P}_F(\omega) + [\mathcal{H}_F(\omega)]^{\dagger}[\mathcal{H}_R(\omega)]\underline{P}_R(\omega). \tag{35}$$

The second term represents the contribution of rigid-body forcing projected onto the retained flexible subspace. As a result, rigid-body forces are absorbed into the flexible estimate, introducing bias. The truncated estimate should therefore be interpreted as an equivalent forcing within the reduced subspace rather than the original modal force components.

2.4. Summary of identifiability implications

The analysis shows that identifiability is governed by the interaction between the sensing operator and the hydroelastic coupling structure. For acceleration-based sensing, all singular values decay uniformly at low frequencies, leading to a global loss of identifiability. For strain-based sensing in the uncoupled case, rigid-body and flexible components remain separated: rigid-body directions are unidentifiable, while flexible directions can be estimated provided the flexible block is well conditioned. When hydroelastic coupling is present, this separation is lost. Rigid-body and flexible modal forces can generate similar strain responses, so that poorly observable directions correspond to coupled force patterns rather than purely rigid-body components. As a result, the inverse problem becomes intrinsically non-identifiable for certain force combinations. Regularization and modal truncation modify these poorly observable directions but do not remove the underlying limitation. Identifiability, variance amplification, and regularization-induced bias is therefore determined by the structure of the structure of the forward operator, rather than by the choice of estimation method.

3. Numerical hydroelastic beam example

Fig. 2 summarizes the workflow of the numerical study and defines the sequence of steps used in this case study. Starting from the hydroelastic model, the forward operator is constructed for a given measurement configuration (acceleration or strain). Synthetic measurements are then generated by applying the forward operator to prescribed modal wave forces and adding measurement noise.

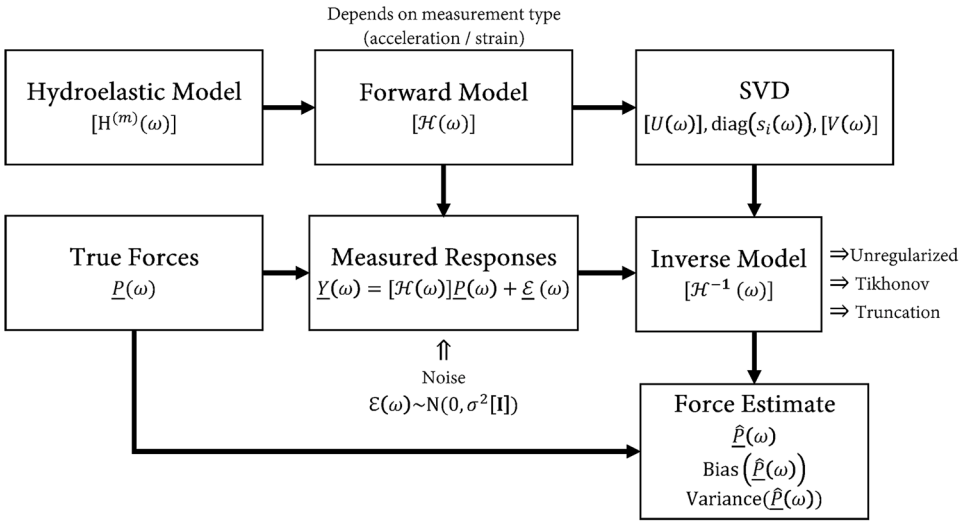

Fig. 2. Workflow of the numerical case study. The hydroelastic model and sensor configuration define the forward operator, which maps modal forces to measured responses. Synthetic measurements are generated by applying the forward operator to prescribed forces and adding noise. The singular value decomposition (SVD) is used to analyse conditioning and identifiability through singular values and singular vectors. The same decomposition is used to construct inverse estimates (unregularized, Tikhonov, and truncated). Analytical expressions for bias and variance are evaluated and compared with individual realizations to interpret estimation performance.

The resulting forward operator is analysed using its singular value decomposition to diagnose conditioning and identifiability, in terms of both singular values and singular directions as explained in Section 2. The same decomposition is then used to construct inverse estimates under different strategies, including the unregularized solution, Tikhonov regularization, and modal truncation. Finally, analytical expressions for the bias and variance of the estimated forces are evaluated and compared with individual realizations, providing a direct link between the theoretical diagnostics in Section 2 and the observed estimation performance.

The hydroelastic model defines the mapping from modal excitation forces to modal responses. Fig. 3 illustrates the construction of the coupled system from the structural and hydrodynamic models. The structure is modeled as a uniform beam of length $L = 200$ m, representative of the scale of a Panamax-class container ship. The beam has a circular cross-section with radius $R = 10$ m and wall thickness $t = 0.0017$ m, with material properties $E = 200$ GPa and $\rho = 1.5 \times 10^6$ kg/m^3. A finite-element model is constructed using 401 Euler–Bernoulli elements and 402 nodes, yielding 804 degrees of freedom. Eight dry modes are retained, including rigid-body and flexible modes, with a uniform modal damping ratio of 0.02.

Hydrodynamic coefficients are computed in the dry modal basis using a boundary element solver [18]. The resulting hydroelastic system exhibits coupling between rigid-body and flexible modes. To demonstrate this, the mode shapes and modal assurance criterion (MAC) matrix are shown in Figs. 4 and 5, respectively. The MAC matrix quantifies the similarity between mode shapes, taking a value of 1 for identical modes and 0 for orthogonal modes. Non-zero off-diagonal values therefore indicate that the wet mode shapes are not orthogonal in the same sense as dry mode shapes, which leads to cross-coupling in the modal frequency response function.

The excitation is defined in terms of modal wave forces, computed for unit-amplitude wave input over a frequency range from 0 to 5 rad/s. These forces represent the true input to the system and are used together with the modal frequency response function to generate the corresponding responses.

The forward operator is constructed from the hydroelastic model and the measurement configuration. The measurement configurations considered in this study are defined in terms of acceleration and strain sensors. Three types of configurations are examined:

- Acceleration-only: $n_a = 8$ sensors
- Strain-only: $n_\epsilon = 8$ sensors
- Mixed configurations: combinations of acceleration and strain sensors, with $n_a = 4$ to 8 and $n_\epsilon = 4$ to 8

All sensor locations are selected to ensure sufficient modal participation, so that the flexible modes are well represented in the measured responses.

Measurement noise is introduced as additive complex Gaussian noise with zero-mean and covariance

$$[\mathbf{\Sigma}_Y] = \begin{pmatrix} \sigma_a^2[\mathbf{I}_a] & 0 \\ 0 & \sigma_\epsilon^2[\mathbf{I}_\epsilon] \end{pmatrix}. \tag{36}$$

The noise levels are chosen to yield comparable signal-to-noise ratios for acceleration and strain measurements.

The singular value decomposition of the forward operator is used as a diagnostic tool, as discussed in Section 2, to identify poorly observable force directions. The same decomposition is used to construct the inverse estimates. Modal forces are estimated

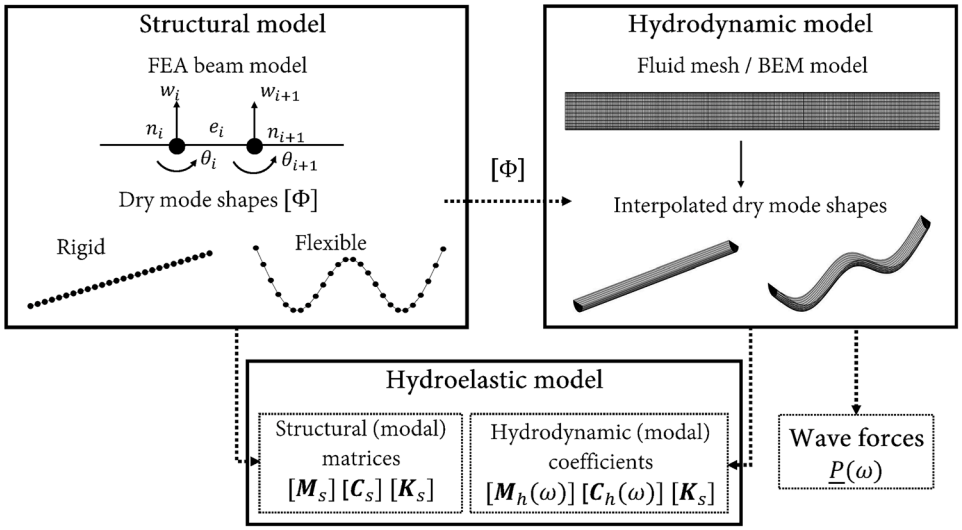

Fig. 3. Schematic representation of the hydroelastic model. A finite-element Euler-Bernoulli beam model with 401 elements is used to construct the dry modal basis, including rigid-body and flexible modes. Hydrodynamic coefficients are computed using a boundary element method (BEM) and projected onto this basis. The resulting hydroelastic model combines structural and hydrodynamic contributions in modal coordinates, defining the frequency response operator that maps modal wave forces to modal responses.

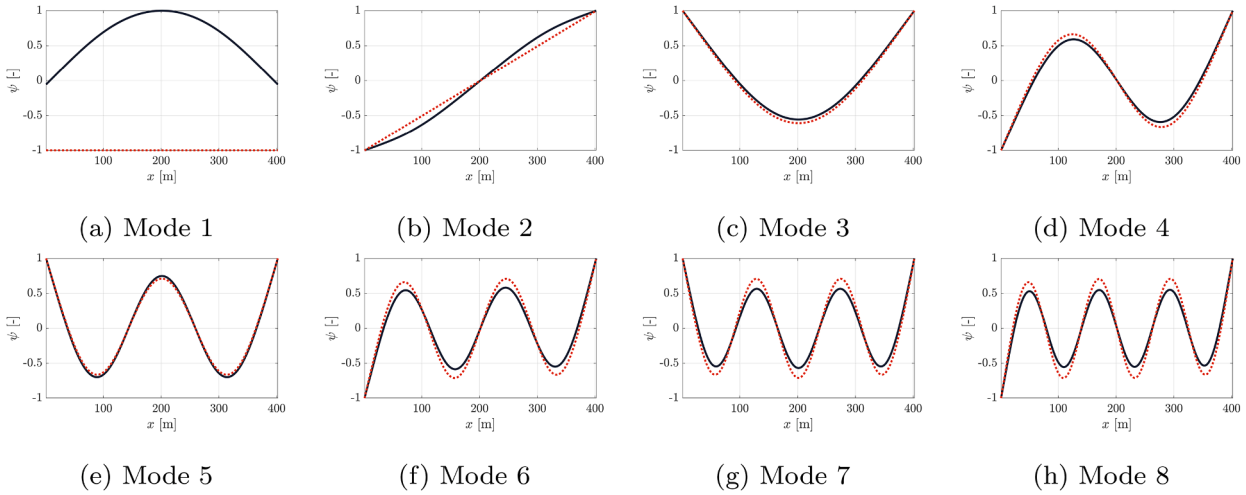

Fig. 4. Mode shapes of Mode 1 - 8 for the dry (solid line) and wet/coupled (dashed line) models.

using different strategies, including the unregularized solution, Tikhonov regularization, and modal truncation. The corresponding analytical expressions for the estimated mean and variance follow directly from the formulation in Section 2.

4. Results

This section examines how sensor type affects the conditioning and identifiability of frequency-domain inverse force estimation in the dry modal basis. Results are presented for three sensor configurations: acceleration-only baseline (Section 4.1), strain-only (Section 4.2), and (mixed acceleration–strain sensing (Section 4.3). The results are interpreted in light of the theoretical framework developed in Section 2, with particular attention to how the singular-value structure of the forward operator governs variance amplification, bias, and the identifiability of rigid-body and flexible force components. Regularization and modal truncation are considered here as illustrative strategies for probing the consequences of poorly observable directions, rather than as remedies for the underlying identifiability limitation.

Unless stated otherwise, the inverse model uses the same modal basis and hydroelastic forward model as the synthetic data generation. Consequently, model errors due to parameter uncertainty are not considered. The only exception is Section 4.2, where

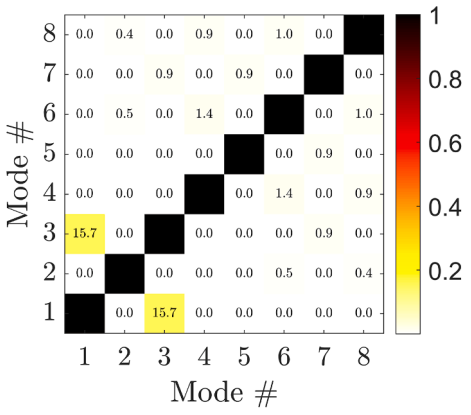

Fig. 5. Modal assurance criterion (MAC) matrix comparing dry and wet mode shapes. Non-zero off-diagonal values indicate coupling between rigid-body and flexible modes in the wet system when expressed in the dry modal basis.

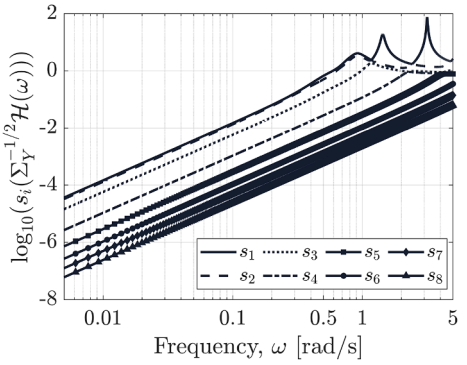

Fig. 6. Singular values of the forward operator for eight acceleration sensors and eight modes.

rigid-body modes are deliberately removed from the inverse basis to examine the effect of excluding the problematic near-null directions.

Note that in several figures, uncertainty bands (blue shading) are included but may not be visually distinguishable where the estimated variance is small relative to the plotted scale.

4.1. Acceleration-only baseline

Acceleration-only sensing provides a useful baseline, as it is known to be ill-conditioned at low frequencies but captures rigid-body motion that cannot typically be observed using strain measurements. Fig. 6 shows the singular values, $s_i(\omega)$ of the whitened acceleration-based forward operator,

$$[\tilde{\mathcal{H}}_a(\omega)] = [\boldsymbol{\Sigma}^{-1/2}][\mathcal{H}_a(\omega)] = [\boldsymbol{\Sigma}^{-1/2}](-\omega^2[\mathbf{S}_a][\mathbf{T}_x][\boldsymbol{\Phi}][\mathbf{H}(\omega)]) = \sum_i s_i(\omega)\,\underline{u}_i(\omega)\,\underline{v}_i(\omega)^H \tag{37}$$

where $[\boldsymbol{\Sigma}]$ is the measurement noise covariance matrix. This whitening ensures that all measurements are weighted according to their noise levels, so that the singular values reflect the noise-normalized conditioning of the inverse problem.

Figs. 7 and 8 compare acceleration-only force estimates without regularization ($\lambda = 0$) and at the optimal regularization level ($\lambda = \lambda^*$). Without regularization, the ensemble means are unbiased, but individual realizations exhibit erratic low-frequency behaviour due to the ill-conditioning of $[\mathcal{H}(\omega)]$, resulting in substantial amplification of measurement noise (high variance). This effect is increasingly pronounced for higher-order modes, for which a broader frequency range is affected by high variance.

The optimal regularization parameter λ^* is selected by minimizing the mean squared error (MSE) of the estimated modal forces,

$$\lambda^* = \arg\min_{\lambda}\ \mathbb{E}\left[\|\underline{\hat{P}}_\lambda(\omega) - \underline{P}(\omega)\|^2\right], \tag{38}$$

where the expectation is evaluated using the analytical expressions for the bias and variance derived in Section 2.

Applying $\lambda = \lambda^*$ suppresses these unstable directions and substantially stabilizes the estimates, particularly for the higher-order modes (Modes 4–8), for which the force spectra are recovered accurately over most of the frequency range above approximately 0.1 rad/s. This improvement is achieved at the cost of bias in frequency bands where the true force is non-negligible. In particular, the pitch force (Modal force 2 in Fig. 8 (b)), which contains significant low-frequency content, is strongly attenuated by regularization.

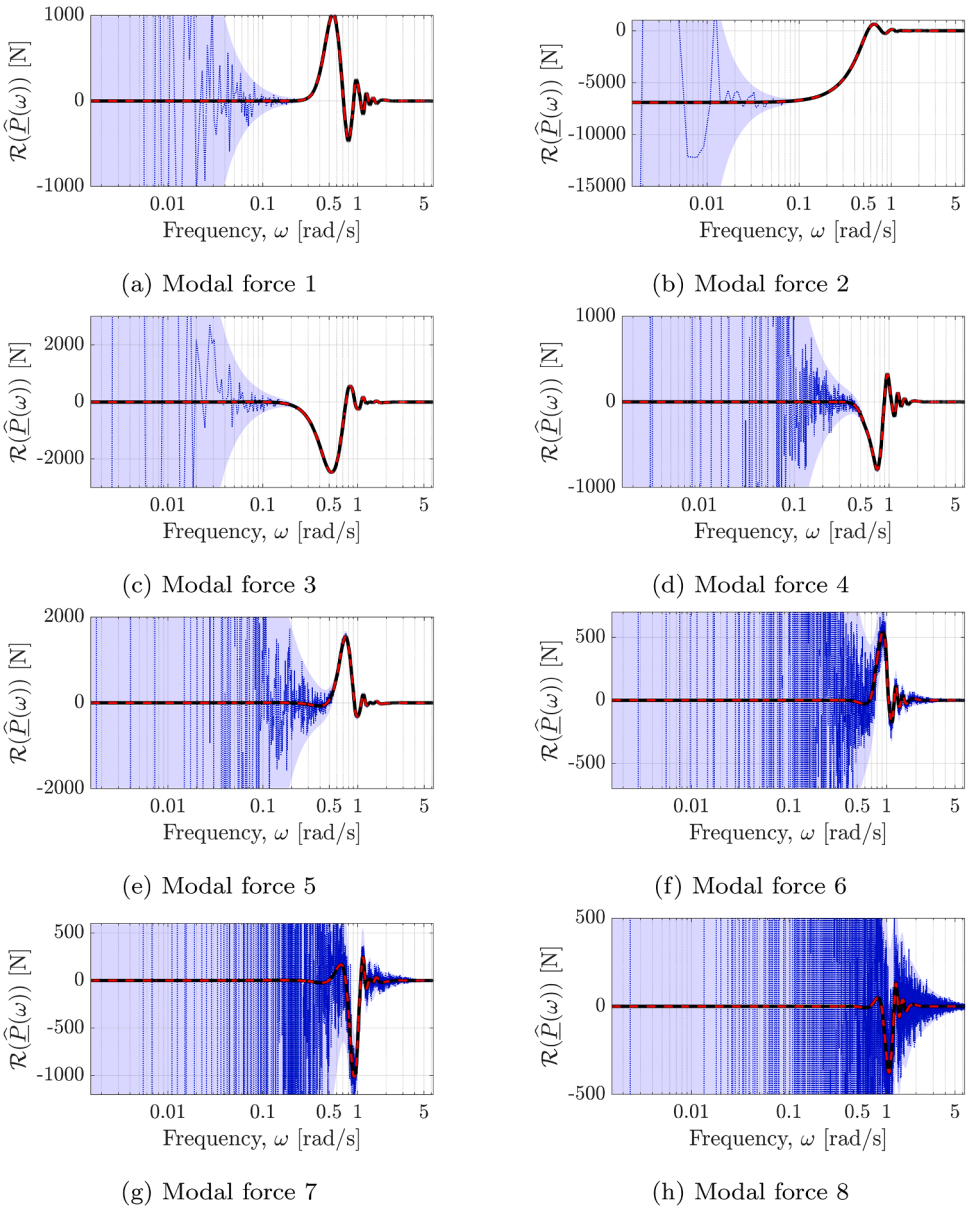

Fig. 7. Acceleration-only force estimates corresponding to Modes 1-8 with $\lambda = 0$. The solid black line denotes the true force; the red dashed line the mean estimate; the blue dotted line a representative single estimate; and the blue shading represents an uncertainty band defined as $\pm 1.96\sigma$ about the mean (not always visible where the variance is small). (For interpretation of the references to colour in this figure legend, the reader is referred to the web version of this article.)

The bias–variance characteristics of the force estimates propagate directly to any reconstructed response quantities, since displacement, velocity, acceleration, and strain are obtained through linear mappings of the estimated modal forces.

Reconstructed response quantities are obtained by applying the corresponding forward operator to the estimated modal forces,

$$\underline{\hat{Y}}_{\mathrm{LOI}}(\omega) = [\mathcal{H}_{\mathrm{LOI}}(\omega)]\, \underline{\hat{P}}(\omega), \tag{39}$$

where $[\mathcal{H}_{\mathrm{LOI}}(\omega)]$ maps modal forces to the response quantity of interest (e.g. displacement, velocity, acceleration, or strain) at the selected location.

Fig. 9 shows the corresponding reconstructed responses at the midspan. Velocity, acceleration, and strain are recovered accurately over most of the band, whereas displacement shows increased low-frequency bias, consistent with the bias in the estimated heave force.

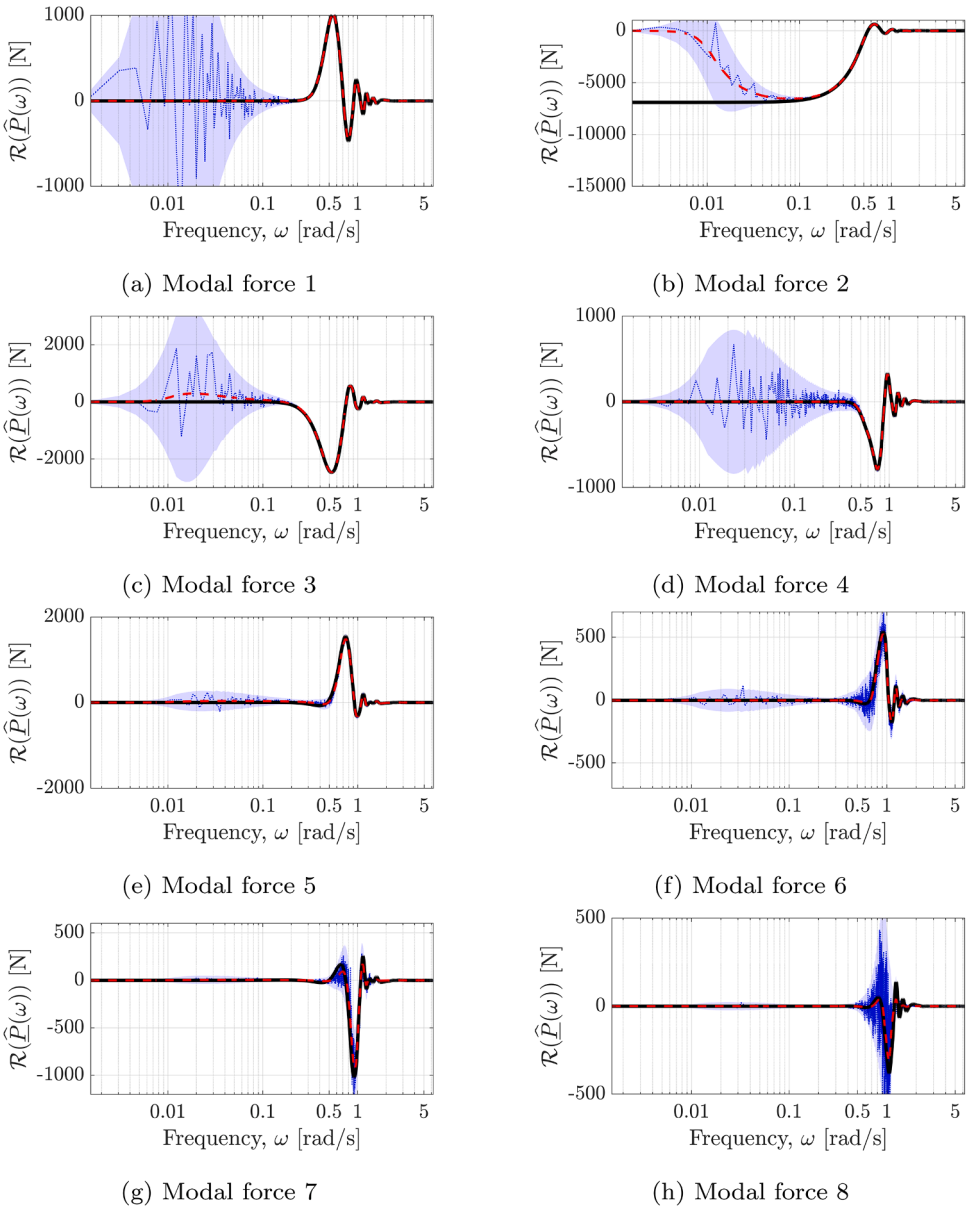

Fig. 8. Acceleration-only force estimates corresponding to Modes 1-8 with $\lambda = \lambda^*$. The solid black line denotes the true force; the red dashed line the mean estimate; the blue dotted line a representative single estimate; and the blue shading represents an uncertainty band defined as $\pm 1.96\sigma$ about the mean (not always visible where the variance is small). (For interpretation of the references to colour in this figure legend, the reader is referred to the web version of this article.)

4.2. Strain-only measurements

Strain measurements are often advocated as a remedy for low-frequency ill-conditioning, as they scale with deformation rather than inertia. We now examine the validity of this assumption when rigid-body modes are included in the inverse force basis.

Fig. 10 shows the singular values of the whitened operator that maps modal forces to strain measurements,

$$[\tilde{\mathcal{H}}_\epsilon(\omega)] = [\boldsymbol{\Sigma}^{-1/2}][\mathcal{H}_\epsilon(\omega)] = [\boldsymbol{\Sigma}^{-1/2}][\mathbf{S}_\epsilon][\mathbf{B}][\boldsymbol{\Phi}][\mathbf{H}^{(m)}(\omega)], \tag{40}$$

where $[\boldsymbol{\Sigma}]$ is the measurement noise covariance matrix. As in Section 4.1, whitening normalizes the measurements by their noise levels, so that the singular values reflect the noise-normalized conditioning of the inverse problem. Fig. 10 shows two singular values remain orders of magnitude smaller than the rest across the full frequency band, indicating a persistent near-null subspace and severe ill-conditioning.

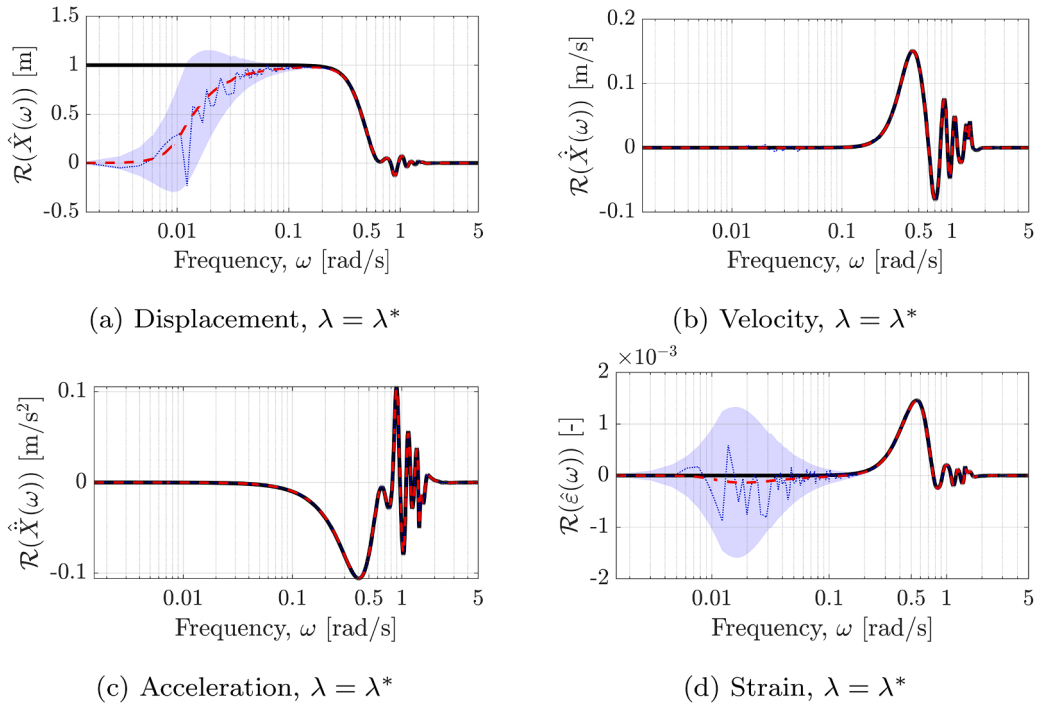

Fig. 9. Estimated spectra for displacement, velocity, acceleration, and strain at the midspan using eight acceleration sensors and an inverse model with eight modes, shown at the optimal regularization level λ^*. The solid black line denotes the true response; the red dashed line the mean estimate; the blue dotted line a representative single estimate; and the blue shading represents an uncertainty band defined as $\pm 1.96\sigma$ about the mean (not always visible where the variance is small). (For interpretation of the references to colour in this figure legend, the reader is referred to the web version of this article.)

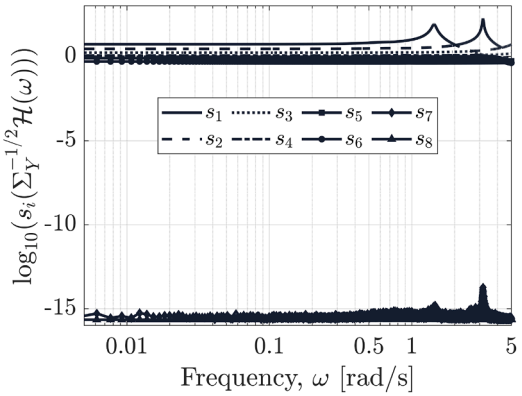

Fig. 10. Singular values of the strain-based forward operator for eight strain sensors and eight estimated modes. Two near-zero singular values persist across the frequency band, indicating a near-null subspace originating from rigid-body modes in the dry basis.

This behaviour is a direct consequence of the dry modal basis: rigid-body modes produce negligible strain ($[\mathbf{B}]\phi_r \approx \mathbf{0}$), so strain-only measurements provide almost no direct sensitivity to the corresponding force directions. Under hydroelastic coupling, these poorly observable directions are no longer purely rigid-body, but involve mixed rigid–flexible combinations. As a result, the loss of observability contaminates multiple force coordinates rather than remaining confined to the rigid-body components.

The impact on force reconstruction is shown in Fig. 11, which reports strain-only modal force estimates for $\lambda = 0$. The least-squares solution exhibits severe noise amplification, with broadband uncertainty extending beyond the rigid-body components. This is consistent with inversion along near-null directions and with the analytical variance expressions derived in Section 2.

To quantify the extent to which each force component is influenced by the near-null directions, we define the *near-null subspace projection energy*. Let

$$[\tilde{H}_\epsilon(\omega)] = [\mathbf{U}(\omega)]\,\mathrm{diag}(s_i(\omega))\,[\mathbf{V}(\omega)]^H \tag{41}$$

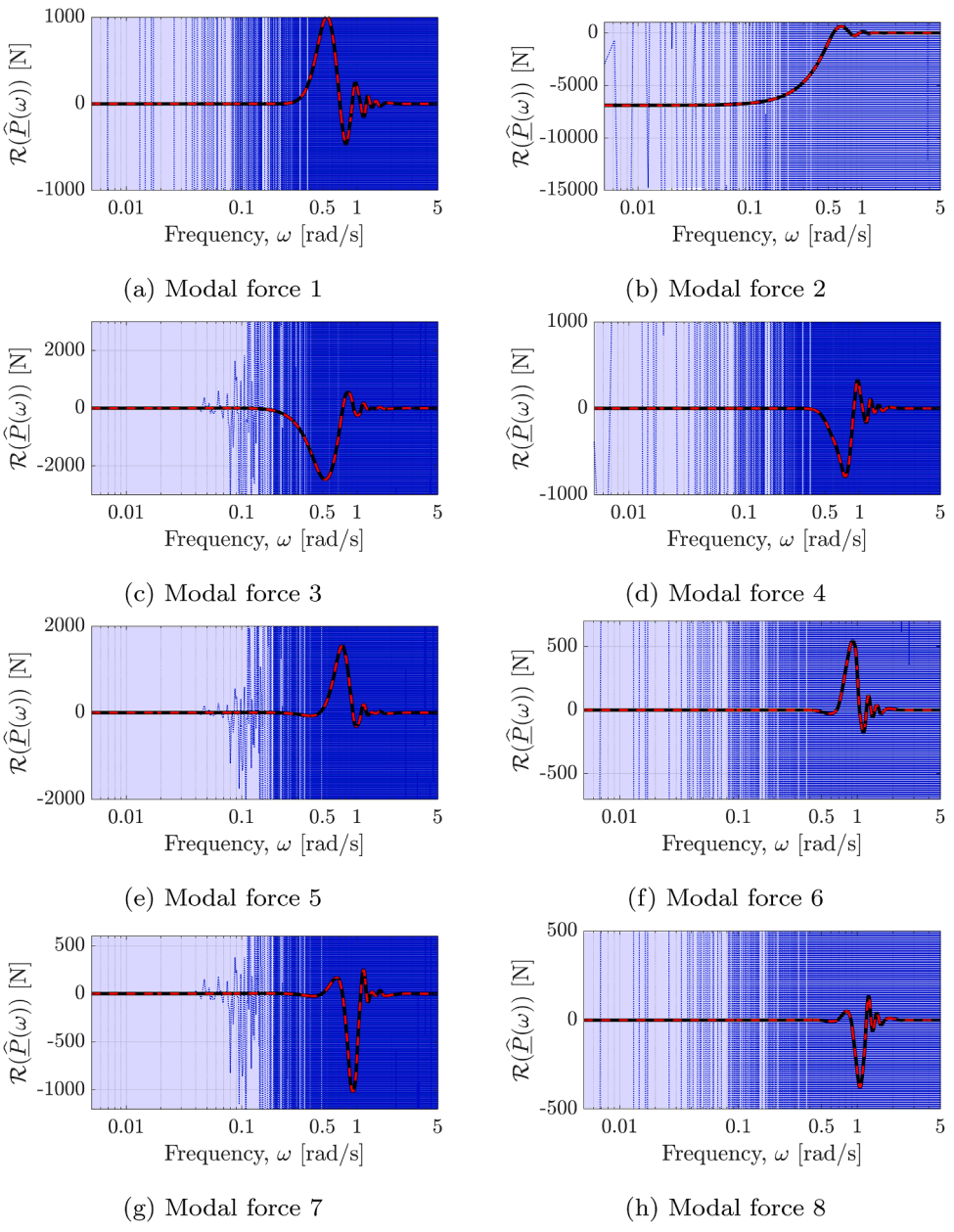

Fig. 11. Strain-only force estimates for Modes 1-8 with $\lambda = 0$. The solid black line denotes the true force; the red dashed line the mean estimate; the blue dotted line a representative single estimate; and the blue shading represents an uncertainty band defined as $\pm 1.96\sigma$ about the mean (not always visible where the variance is small). (For interpretation of the references to colour in this figure legend, the reader is referred to the web version of this article.)

denote the singular value decomposition of $[\tilde{H}_\epsilon(\omega)]$. Based on Fig. 10, we define the near-null subspace as $\mathcal{B}(\omega) = \text{span}\{v_7(\omega), v_8(\omega)\}$. The near-null projection energy of force component j is then

$$E_{j,\mathcal{B}}(\omega) = |V_{j7}(\omega)|^2 + |V_{j8}(\omega)|^2. \tag{42}$$

Values of $E_{j,\mathcal{B}}(\omega)$ near 1 indicate that a force component is strongly aligned with the near-null directions and is therefore expected to exhibit large variance in unregularized estimates.

Fig. 12 shows $E_{j,\mathcal{B}}(\omega)$ for all force components. At low frequencies, the near-null subspace is dominated by rigid-body directions, while several flexible components exhibit increasing projection energy with frequency. This confirms that hydroelastic coupling causes the poorly observable directions to evolve into mixed rigid–flexible combinations, which explains the broadband ill-conditioning of the unregularized strain-only estimates.

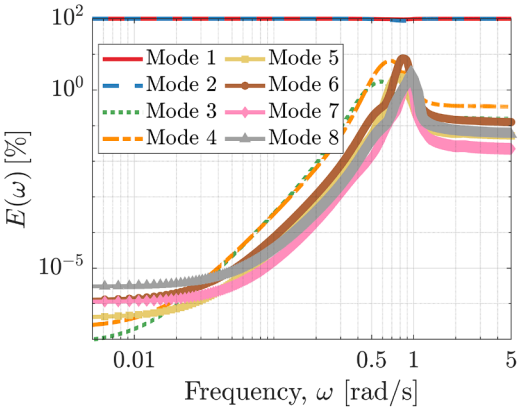

Fig. 12. Near-null subspace projection energy $E_{j,\mathcal{B}}(\omega) = |V_{j7}(\omega)|^2 + |V_{j8}(\omega)|^2$ for each force component, computed from the SVD of the strain-based forward operator. Growth of $E_{j,\mathcal{B}}(\omega)$ for Modes 3–8 indicates frequency-dependent mixing of rigid and flexible directions under wet coupling.

Fig. 13 shows the corresponding force estimates under best-case regularization ($\lambda = \lambda^*$). Regularization suppresses the contribution of the near-null directions and substantially reduces variance relative to $\lambda = 0$. However, rigid-body forces are biased in the frequency range where the true forces are non-negligible, reflecting that strain measurements contain insufficient information to uniquely identify rigid-body forcing. Bias is also observed in flexible modes at frequencies where $E_{j,\mathcal{B}}(\omega)$ is large, confirming that regularization stabilizes the inversion but cannot recover force content aligned with the near-null subspace.

A natural response is to remove the rigid-body modes from the inverse basis and estimate only the flexible components. Doing so eliminates the dominant near-null directions and yields a reduced inverse problem that is well conditioned without the need for explicit regularization.

Fig. 14 shows strain-only force estimates obtained using this truncated inverse, in which only Modes 3–8 are retained and $\lambda = 0$. Compared to the full-basis strain-only results (Figs. 11–13), the estimates are substantially stabilized across the frequency range. This stabilization occurs because truncation removes the poorly observable rigid-body directions, preventing the inversion from exciting the near-null subspace responsible for severe noise amplification.

The reduction in variance is accompanied by bias, since the inverse problem must represent the effects of rigid-body forcing using only the retained flexible subspace. The resulting coefficients should therefore be interpreted as surrogate forcing coordinates rather than as physical modal forces. In this sense, modal truncation acts as a hard subspace constraint, whereas Tikhonov regularization retains the full basis and attenuates poorly observable directions continuously.

The implications of this re-parameterization become clearer when reconstructing response quantities at the locations of interest. Figs. 15 and 16 compare reconstructed displacement, velocity, acceleration, and strain for the regularized full-basis inverse and the unregularized truncated inverse, respectively.

In the full-basis case, regularization reduces variance but introduces noticeable bias in the reconstructed responses, particularly at low frequencies where rigid-body forcing dominates and is weakly observable from strain measurements. In the truncated case, the retained flexible modes still reproduce the deformation-driven strain response well, so the reconstructed strain remains accurate. However, displacement, velocity, and acceleration retain noticeable bias because the rigid-body contribution has been removed from the inverse basis and cannot be recovered explicitly. The truncated inverse therefore improves stability and preserves strain reconstruction, but it does not provide accurate reconstruction of response quantities that depend strongly on the missing rigid-body content.

4.3. Mixed acceleration–strain measurements

Mixed acceleration–strain sensing is considered to combine information from global motion (accelerations) and deformation (strain). Fig. 17 shows that adding strain sensors produces six well-conditioned singular values associated with flexible-mode forcing over most of the band, while two singular values remain acceleration-dominated and collapse as $\omega \to 0$. Therefore, mixed sensing can substantially improve observability of flexible forcing, but it cannot remove the intrinsic low-frequency ill-conditioning associated with rigid-body motion.

Because strain measurements are insensitive to rigid-body motion, mixed sensing does not fundamentally change the identifiability of rigid-body force components. Instead, it redistributes estimator variance across frequency and across force components: rigid-body forces remain acceleration-dominated at low frequencies, while flexible-mode forces benefit from strain sensitivity at higher frequencies.

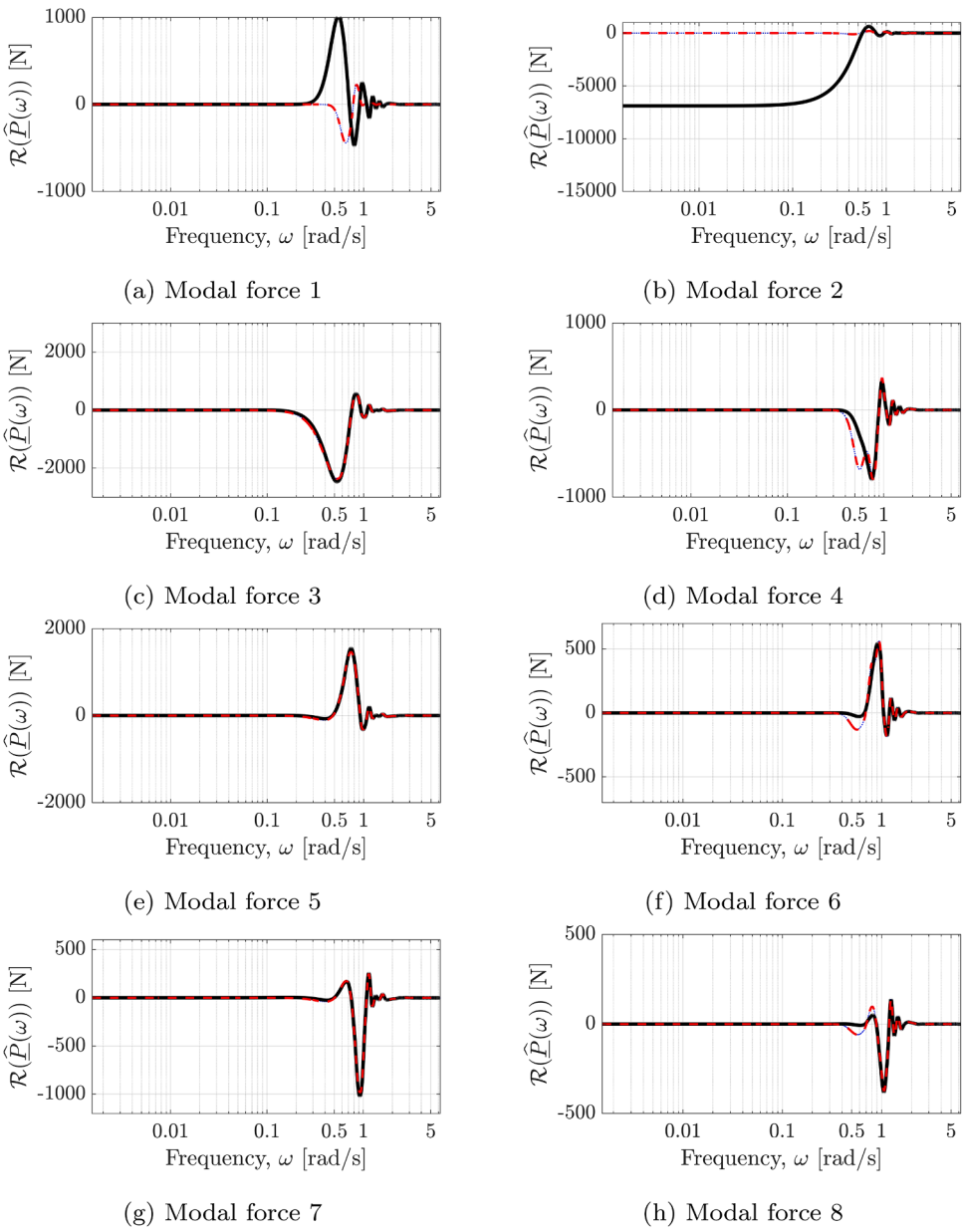

Fig. 13. Strain-only force estimates for Modes 1-8 with $\lambda = \lambda^*$. The solid black line denotes the true force; the red dashed line the mean estimate; the blue dotted line a representative single estimate; and the blue shading represents an uncertainty band defined as $\pm 1.96\sigma$ about the mean (not always visible where the variance is small). (For interpretation of the references to colour in this figure legend, the reader is referred to the web version of this article.)

To summarize estimation performance across configurations, we report the total mean-squared error (TMSE) and TMSE per modal force component,

$$\mathrm{TMSE}_r = \sum_{\omega} \mathrm{MSE}\big(\hat{P}_r(\omega)\big). \tag{43}$$

Fig. 18 shows that increasing the number of strain sensors substantially reduces TMSE for the flexible components (Modes 3–8), consistent with the improved conditioning in Fig. 17. In contrast, the rigid-body components (Modes 1–2) show comparatively limited improvement because strain measurements contain negligible direct information about rigid-body motion.

Figs. 19 and 20 illustrate the practical implication using unregularized estimates ($\lambda = 0$) for two representative configurations: A4 + S8 (sufficient strain sensing) and A8 + S4 (insufficient strain sensing). For the flexible component shown (Modal force 6), A4 + S8 yields a stable estimate with substantially reduced variance, whereas A8 + S4 remains noisy. For the rigid-body-dominated component

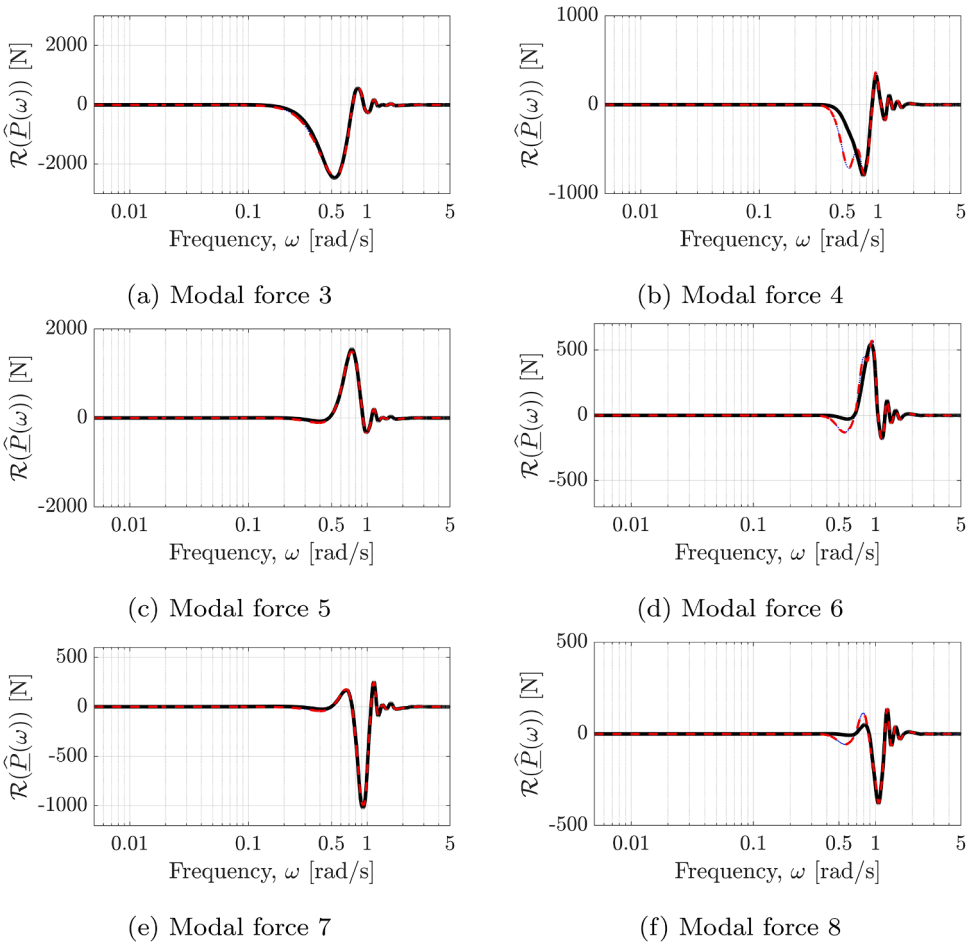

Fig. 14. Strain-only force estimates for Modes 3–8 after removing rigid-body modes from the inverse basis (unregularized, $\lambda = 0$). The solid black line denotes the true force; the red dashed line the mean estimate; the blue dotted line a representative single estimate; and the blue shading represents an uncertainty band defined as $\pm 1.96\sigma$ about the mean (not always visible where the variance is small). (For interpretation of the references to colour in this figure legend, the reader is referred to the web version of this article.)

(Modal force 1), both configurations retain elevated low-frequency uncertainty, consistent with the two acceleration-dominated singular values in Fig. 17.

4.4. Summary of findings

The main observations are:

- Acceleration-only inversion becomes ill-conditioned at low frequencies; regularization stabilizes the solution but introduces bias in frequency bands where the true force is non-negligible.
- Strain-only inversion using a dry modal basis that includes rigid-body modes exhibits a near-null subspace, rendering rigid-body force components unidentifiable from strain measurements regardless of regularization.
- Removing rigid-body modes from the inverse basis stabilizes strain-only force estimation and preserves accurate reconstruction of deformation-driven strain responses, but displacement, velocity, and acceleration remain biased because the rigid-body contribution is excluded. The resulting force estimates represent equivalent forcing in a reduced flexible subspace rather than physical modal forces.
- Mixed acceleration–strain sensing substantially improves estimation of flexible-mode forces, while rigid-body force components remain poorly conditioned at low frequencies because strain measurements provide negligible direct information about rigid-body motion.

Although these results are demonstrated using a simplified hydroelastic beam model, the observed behaviour is not specific to this example. The loss of identifiability arises from the interaction between the sensor type and the modal representation, and therefore

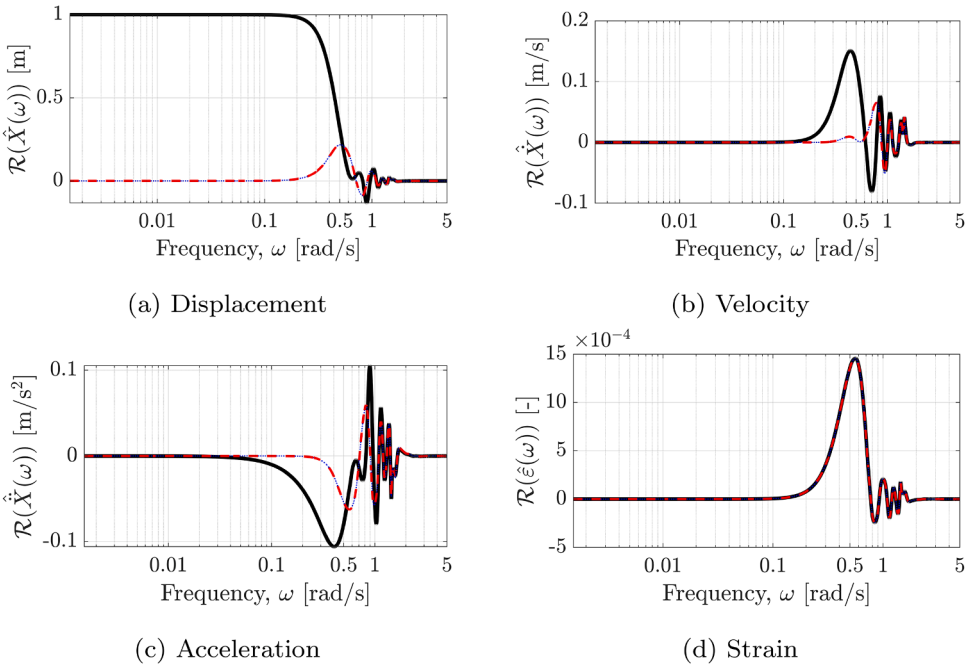

Fig. 15. Estimated spectra for displacement, velocity, acceleration, and strain at the midspan LOIs using eight strain sensors and the full eight-mode inverse basis, shown at the best-case regularization level $\lambda = \lambda^*$. The solid black line denotes the true response; the red dashed line the mean estimate; the blue dotted line a representative single estimate; and the blue shading represents an uncertainty band defined as $\pm 1.96\sigma$ about the mean (not always visible where the variance is small). (For interpretation of the references to colour in this figure legend, the reader is referred to the web version of this article.)

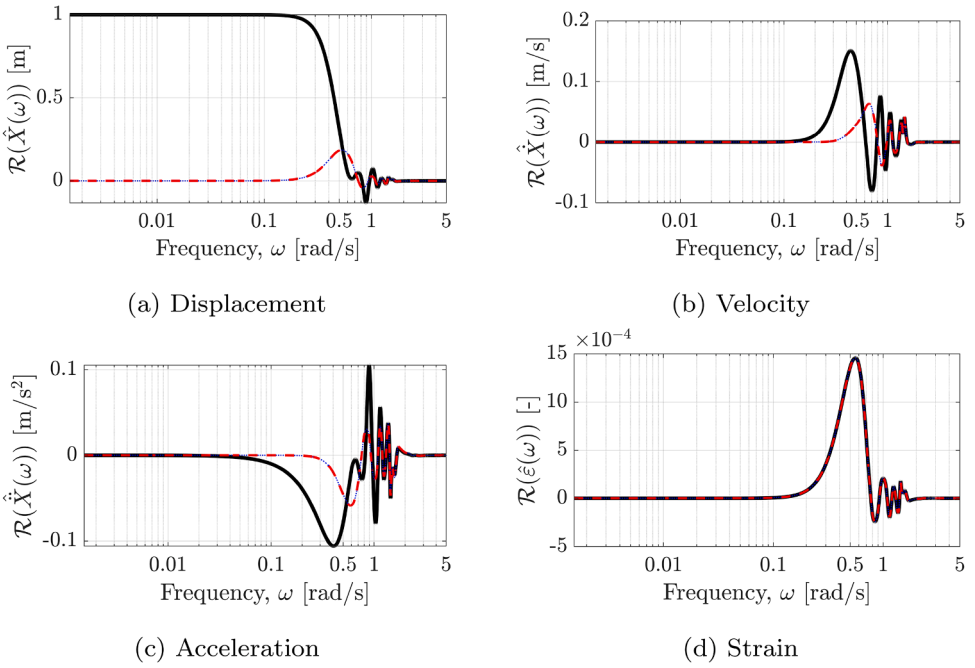

Fig. 16. Estimated spectra for displacement, velocity, acceleration, and strain at the midspan LOIs using eight strain sensors and a truncated inverse basis (Modes 3–8), shown without regularization ($\lambda = 0$). The solid black line denotes the true response; the red dashed line the mean estimate; the blue dotted line a representative single estimate; and the blue shading represents an uncertainty band defined as $\pm 1.96\sigma$ about the mean (not always visible where the variance is small). (For interpretation of the references to colour in this figure legend, the reader is referred to the web version of this article.)

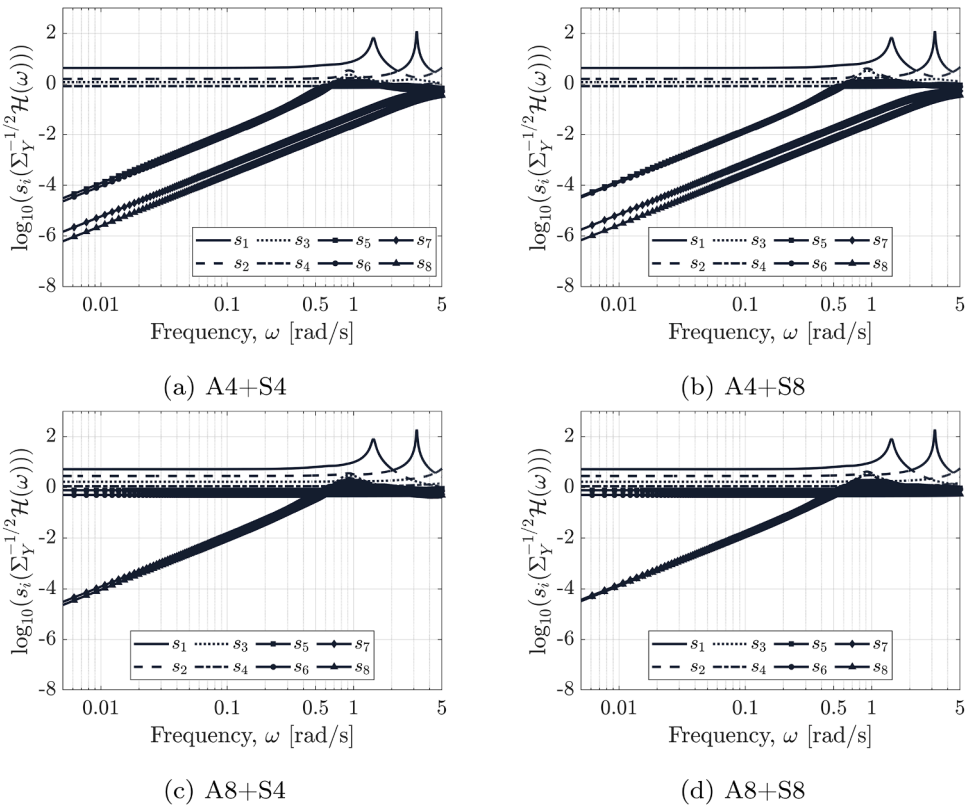

Fig. 17. Singular values of the mixed-sensing forward operator (eight modes). Six strain-informative directions (flexible content) remain well conditioned, whereas two rigid-body-dominated directions remain poorly conditioned as $\omega \to 0$ because only accelerometers carry information about rigid-body motion.

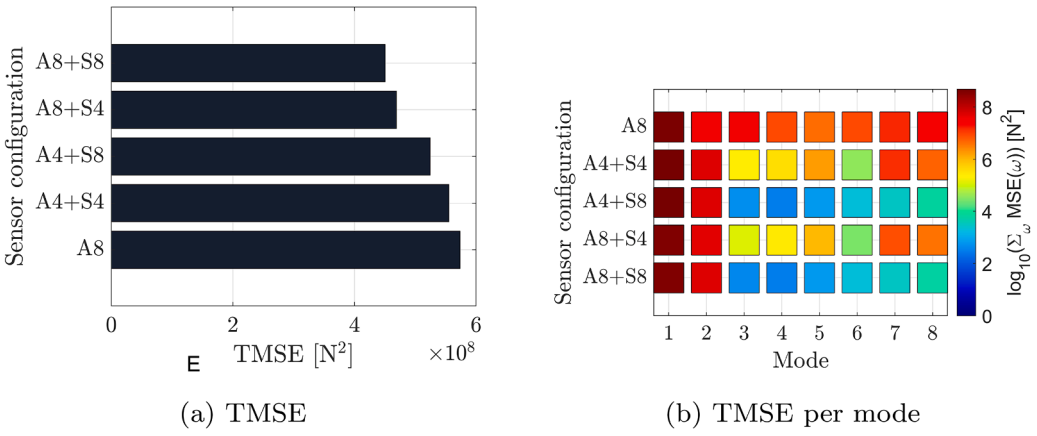

Fig. 18. TMSE metrics for mixed sensing (eight modes). Adding strain sensors reduces error primarily in the flexible components (Modes 3–8), while rigid-body components (Modes 1–2) remain sensitive to low-frequency ill-conditioning.

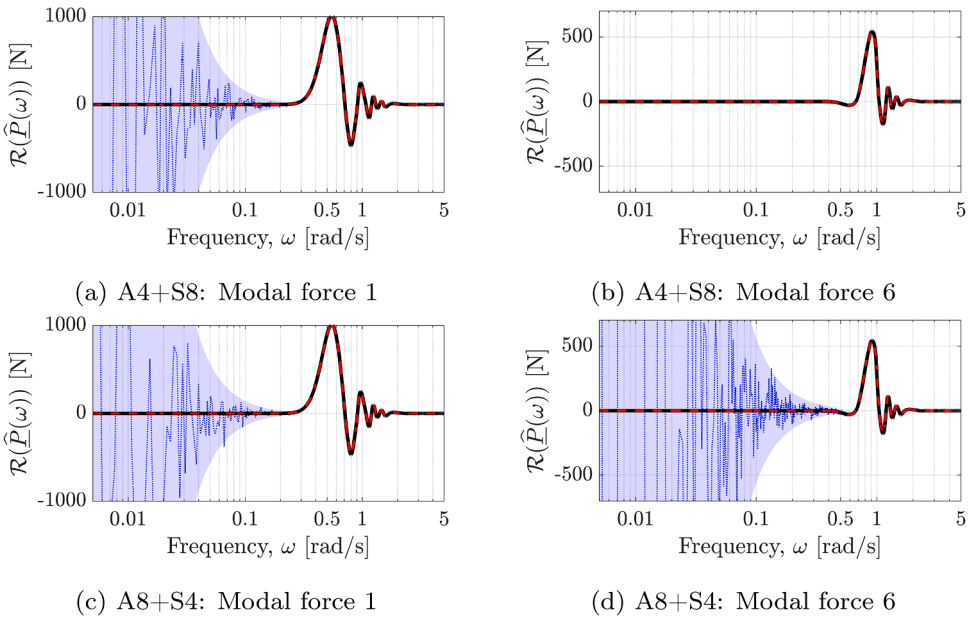

(a) A4+S8: Modal force 1

(b) A4+S8: Modal force 6

(c) A8+S4: Modal force 1

(d) A8+S4: Modal force 6

Fig. 19. Representative unregularized ($\lambda = 0$) modal force estimates for mixed sensing. With sufficient strain sensing (A4 + S8), variance is strongly reduced for flexible components (e.g. Modal force 6), while rigid-body components (e.g. Modal force 1) remain poorly conditioned at low frequencies. The solid black line denotes the true force; the red dashed line the mean estimate; the blue dotted line a representative single estimate; and the blue shading represents an uncertainty band defined as $\pm 1.96\sigma$ about the mean (not always visible where the variance is small). (For interpretation of the references to colour in this figure legend, the reader is referred to the web version of this article.)

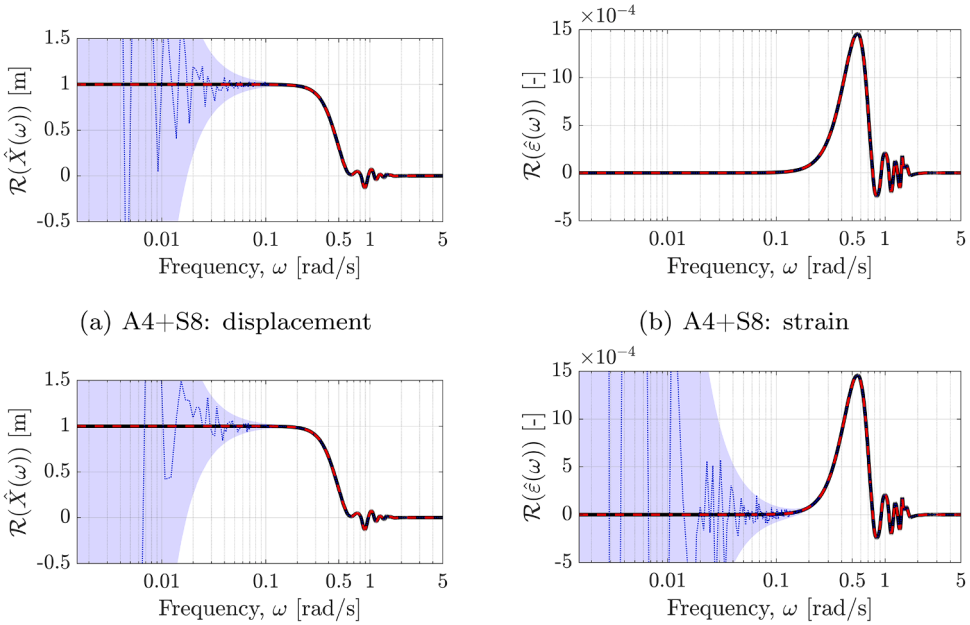

(a) A4+S8: displacement

(b) A4+S8: strain

(c) A8+S4: displacement

(d) A8+S4: strain

Fig. 20. Representative unregularized ($\lambda = 0$) reconstructions at the midspan LOI for mixed sensing. Strain is recovered accurately when sufficient strain sensors are available (A4 + S8), while low-frequency displacement remains sensitive to rigid-body ill-conditioning because rigid-body forcing is primarily informed by acceleration measurements. The solid black line denotes the true force; the red dashed line the mean estimate; the blue dotted line a representative single estimate; and the blue shading represents an uncertainty band defined as $\pm 1.96\sigma$ about the mean (not always visible where the variance is small). (For interpretation of the references to colour in this figure legend, the reader is referred to the web version of this article.)

applies more generally to flexible structures where rigid-body and deformation modes are coupled. The example serves to illustrate this structural limitation in a controlled setting.

5. Conclusions

This study focused on developing qualitative insight into how sensor type and modelling choices influence the conditioning of inverse force estimation for hydroelastic systems. This perspective is particularly relevant for floating structures, whose dynamics are dominated by low-frequency rigid-body motion coupled with flexible deformation-precisely the regime in which inverse formulations are most prone to ill-conditioning and noise amplification.

The central finding of this work is that strain-based inverse formulations fundamentally fail to identify rigid-body force components when a dry modal basis containing rigid-body modes is used. Because rigid-body motion produces negligible strain, the corresponding force components lie in (or close to) the null space of the strain-based forward operator. This limitation is structural and cannot be resolved through regularization, optimal parameter tuning, or alternative estimation techniques such as Bayesian or Kalman-filter-based methods. Regularization therefore serves primarily to expose the bias–variance consequences of poor observability, rather than to overcome the underlying limitation itself.

A naive regularization strategy is to remove rigid-body modes from the inverse model, which redistributes rigid-body content into flexible coordinates and yields surrogate force estimates in the reduced subspace. While this can stabilize the inversion and preserve accurate reconstruction of deformation-driven strain responses, it also introduces bias in displacement, velocity, and acceleration, since the rigid-body contribution is no longer represented explicitly.

Acceleration-based measurements, in contrast, do contain information about rigid-body motion, but inverse problems formulated using accelerations are strongly ill-conditioned at low frequencies. Regularization can stabilize the solution, but when rigid-body forces are significant in this frequency range, variance reduction is achieved at the cost of bias.

Combining acceleration and strain measurements offers a practical compromise. Strain sensors provide robust information about flexible modes across a wide frequency range, while accelerometers are essential for capturing rigid-body motion. Mixed sensing substantially improves identifiability and reduces estimation error for flexible-mode forces and deformation-driven responses. However, rigid-body force components remain poorly conditioned at low frequencies, reflecting the fact that only acceleration measurements carry information about these modes in the adopted formulation.

Overall, the results highlight that limitations in inverse force estimation for hydroelastic systems arise from the structure of the inverse problem itself rather than from deficiencies in specific algorithms or parameter choices. These findings underscore the need for careful alignment between sensor type, modal basis, and estimation objectives. More broadly, the conclusions extend beyond marine structures to any inverse problem that combines modal reduction with strain-based sensing in the presence of rigid or quasi-rigid modes.

The present study is restricted to linear dynamics with known system parameters; uncertainty in structural and hydrodynamic properties was not considered. While such uncertainties are important in practice, the results demonstrate that even under idealized conditions and best-case regularization, fundamental identifiability limits persist.

Declaration of generative AI and AI-assisted technologies in the manuscript preparation process

During the preparation of this work the author(s) used ChatGPT 5 in order to improve readability of the text. After using this tool/service, the authors reviewed and edited the content as needed and take full responsibility for the content of the published article.

CRediT authorship contribution statement

Christof Van Zijl: Writing – original draft, Visualization, Validation, Software, Project administration, Methodology, Investigation, Formal analysis, Data curation, Conceptualization; **Jovana Jovanova:** Writing – review & editing, Supervision, Resources, Funding acquisition, Conceptualization; **Apostolos Grammatikopoulos:** Writing – review & editing, Supervision, Resources, Project administration, Funding acquisition, Conceptualization.

Data availability

Data will be made available on request.

Declaration of competing interest

The authors declare that they have no known competing financial interests or personal relationships that could have appeared to influence the work reported in this paper.

Acknowledgements

The authors would like to thank Delft University of Technology for enabling this research as a project awarded by the faculty of Mechanical Engineering.

References

[1] A. Gallet, S. Rigby, T.N. Tallman, X. Kong, I. Hajirasouliha, A. Liew, D. Liu, L. Chen, A. Hauptmann, D. Smyl, et al., Structural engineering from an inverse problems perspective, Proc. R. Soc. A Math. Phys. Eng. Sci. 478 (2257) (2022) 20210526. https://doi.org/10.1098/rspa.2021.0526

[2] K.L. Yu, K.E. Tatsis, V.K. Dertimanis, E.N. Chatzi, A.W. Smyth, et al., A spatio-temporal model for response and distributed wave load estimation on offshore wind turbines, in: R. Platz, G. Flynn, K. Neal, S. Ouellette (Eds.), Model Validation and Uncertainty Quantification, Volume 3, Springer Nature Switzerland, Cham, 2024, pp. 133–140. Series Title: Conference Proceedings of the Society for Experimental Mechanics Series, https://doi.org/10.1007/978-3-031-37003-8_21

[3] L. Caglio, A. Sadeqi, H. Stang, E. Katsanos, et al., Joint input-state estimation of structures subjected to complex loads via augmented Kalman filter with physics informed latent force models, Mech. Syst. Signal Process. 223 (2025) 111852. https://doi.org/10.1016/j.ymssp.2024.111852

[4] E. Jacquelin, A. Bennani, P. Hamelin, et al., Force reconstruction: analysis and regularization of a deconvolution problem, J. Sound Vib. 265 (1) (2003) 81–107. https://doi.org/10.1016/S0022-460X(02)01441-4

[5] J. Sanchez, Mathematical examination of force reconstruction and the deconvolution problem, Results Eng. 14 (2022) 100391. https://doi.org/10.1016/j.rineng.2022.100391

[6] K. Maes, E. Lourens, K. Van Nimmen, E. Reynders, G. De Roeck, G. Lombaert, et al., Design of sensor networks for instantaneous inversion of modally reduced order models in structural dynamics, Mech. Syst. Signal Process. 52-53 (2015) 628–644. https://doi.org/10.1016/j.ymssp.2014.07.018

[7] E. Lourens, D.J.M. Fallais, Full-field response monitoring in structural systems driven by a set of identified equivalent forces, Mech. Syst. Signal Process. 114 (2019) 106–119. https://doi.org/10.1016/j.ymssp.2018.05.014

[8] H.M. Alqam, A.K. Dhingra, Frequency response-based indirect load identification using optimum placement of strain gages and accelerometers, J. Vib. Acoust. 141 (031013) (2019). https://doi.org/10.1115/1.4042709

[9] R.E.D. Bishop, W.G. Price, Y. Wu, et al., A general linear hydroelasticity theory of floating structures moving in a seaway, Philos. Trans. R. Soc. London, Ser. A Math. Phys. Sci. 316 (1538) (1986) 375–426. Publisher: Royal Society,

[10] Y.-S. Wu, W.-C. Cui, et al., Advances in the three-dimensional hydroelasticity of ships, Proc. Inst. Mech. Eng. M J. Eng. Marit. Environ. 223 (3) (2009) 331–348. https://doi.org/10.1243/14750902JEME159

[11] S.E. Hirdaris, P. Temarel, Hydroelasticity of ships: recent advances and future trends, Proc. Inst. Mech. Eng. M J. Eng. Marit. Environ. 223 (3) (2009) 305–330. https://doi.org/10.1243/14750902JEME160

[12] A.N. Tikhonov, Regularization of incorrectly posed problems, Sov. Math. Dokl. 4 (1963) 1624–1627. https://sid.ir/paper/535585/en

[13] E. Lourens, E. Reynders, G. De Roeck, G. Degrande, G. Lombaert, et al., An augmented Kalman filter for force identification in structural dynamics, Mech. Syst. Signal Process. 27 (2012) 446–460. https://doi.org/10.1016/j.ymssp.2011.09.025

[14] E. Zhang, J. Antoni, P. Feissel, et al., Bayesian force reconstruction with an uncertain model, J. Sound Vib. 331 (4) (2012) 798–814. https://doi.org/10.1016/j.jsv.2011.10.021

[15] C. Yang, Q. Shi, B. Lin, K. Hu, F. Zhu, et al., Regularization method for load reconstruction with hybrid uncertainties based on interval theory and convex model theory, J. Sound Vib. 619 (2025) 119389. https://doi.org/10.1016/j.jsv.2025.119389

[16] C. Yang, Q. Yu, Multi-objective optimization-inspired set theory-based regularization approach for force reconstruction with bounded uncertainties, Comput. Methods Appl. Mech. Eng. 438 (2025) 117814. https://doi.org/10.1016/j.cma.2025.117814

[17] C. Yang, Load-dependent structural state reconstruction-oriented and reliability-based sensor placement optimization method, AIAA J. (2025) 1–12. https://doi.org/10.2514/1.J065285

[18] M. Ancellin, F. Dias, et al., Capytaine: a Python-based linear potential flow solver, J. Open Source Softw. 4 (36) (2019) 1341. https://doi.org/10.21105/joss.01341